Why are Tensile Cracks Suppressed under Dynamic Loading? – Transition Strain Rate for Failure Mode

Chunjiang Zou[1*], Jianchun Li[2*], Xiaobao Zhao[3], Jian Zhao[1]

[1*]Department of Civil Engineering, Monash University, Australia

[2*]School of Civil Engineering, Southeast University, China

[3]School of Earth Sciences and Engineering, Nanjing University, China

Corresponding author: Chunjiang Zou (chunjiang.zou@monash.edu); Jianchun Li (jcli@seu.edu.cn)

Abstract

Mechanical properties of rocks under dynamic loading are significantly different from those under quasi-static loading. This difference is driven by more fundamental mechanical principles of materials at failure and will influence subsequent macroscale cracking behaviour. Understandings on this fundamental mechanism, however, are still controversial significantly. This paper tries to provide a feasible explanation of the underlying connections between the rate-dependent strength and the cracking behaviours. Open-flaw marble specimens, which provide good stress concentration at possible fracture initiation and material homogeneity, have been investigated experimentally and mathematically. We observe that experimentally the tensile strength is more sensitive to strain rate than the compressive strength. Meanwhile, tensile cracks are suppressed under dynamic loading, while shear cracks appear first along the flaw boundary. We incorporate the "localized strain rate effect" concept into the analytical study and propose the "transition strain rate" as a watershed for the different fracturing behaviours under quasi-static and dynamic loadings. This model successfully explains why the tensile cracks are suppressed in rocks under dynamic loading, while quasi-statically, the stress

distribution nonuniformity would suggest otherwise cracking behaviours. The well-correlation between the experimental and modelling results indicates that the model can be introduced to quantitatively analyze more complex macroscopic problems involving high strain rates in material science, geology and civil engineering.

Keywords: dynamics, strength, strain rate, flaw, stress concentration, crack

Highlights:

1. Proposing universal explanation on suppression of tensile failure under dynamic loading
2. Theoretical model bridges elementary dynamic strength hardening with crack development
3. Proposing and evaluating local strain rate effect and localized strength
4. Giving analytical solution for transition strain rate of failure mode

1 Introduction

Earthquake, meteorite impact, underground engineering, mining activities usually involve very high-rate loadings ranging typically from 10 to 10^4 s^{-1} or even higher [1-3]. In earthquakes, the slip rate of the fault can be as high as 4 m/s [4], which implies for a particular activated section on a slipping fault, the shear strain rate might be higher than 1 to 10 s^{-1}. Besides the slipping dynamics, the strain rate of shake loading near the earthquake epicentre can be 10^3 to 10^4 s^{-1} [5]. Asteroid impact on a solid planet is another common issue concerning rock dynamics. The strain rate at the impact centre can be as high as 10^9-10^{12} s^{-1} and cause the high plasticity, melting and crystal phase transformation [6, 7]. Since this strain rate decays rapidly with the distance, the dynamic strain rate of the most affected region should be less than 10^3 s^{-1}. Rock masses are not homogeneous but containing inherent defects such as flaws, fractures, joints, caves, water or faults. The high loading rates generated from those above mentioned natural scenarios will significantly change the mechanical properties and fracturing process of

rocks and then change the failure mode of geological bodies, as illustrated in **Figure 1**. In the mesoscopic and microscopic view, the rock contains a large number of randomly oriented weak or damaged zones in the forms of voids, weak lens, weak grains and grain boundaries. These heterogeneities and randomness impart the rock failure process of inherent complexity from the very fundamental scales.

The cracking behaviour of rocks is influenced by the loading rate or loading conditions based on plenty of natural and experimental observations. Dynamic loadings usually produce higher number of cracks which induces fine fragments and more favoured compressive failure, e.g. fragmentation [2, 3, 8] and spalling phenomena[9]. Shear cracks are observed to be more favoured under dynamic loadings than tensile cracks under quasi-static loadings [10, 11]. The crack high loading rates in steel shows a distinct propagation direction with a shiny, mirror-like smeared-over crack surface [12]. "At very high loading rates, damage is obviously no longer caused by a fracture process but by a localized shear band process" [12]. A similar phenomenon is also observed in rock, polymer and alloy in macroscopic and microscopic scales [13-16]. The X-shaped shear failure mode is also observed in the quartz grains of rock in quartz grains from the crater-fill breccia unit of the Decorah impact structure by a meteorite impact event [16] (**Figure 1**). Failure mode transforms when the impact speed or the dynamic loading rate reaches a certain speed. The transition speed varies with the notch tip bluntness [17]. For the notched specimen in polycarbonate under dynamic loading of pure shear, when increasing the impact speed from 20 to 55 m/s, the crack initiation changes from tensile mode-1 to pure shear, and the crack propagation direction also changes significantly [13, 15]. For the Carrara marble and gypsum, such transition of failure mode is also observed[10, 11].

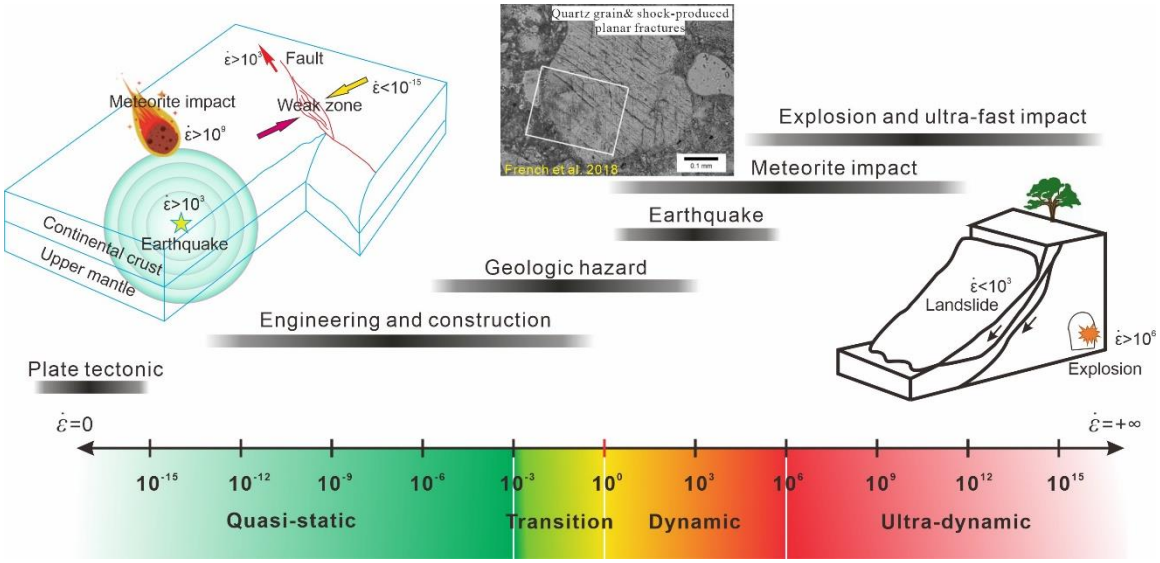

Figure 1. Typical strain rate ranges in different geological cases (The photo of the X-shape fractures in quartz grains produced by meteorite impact is give by French et al. 2018[16])

The strain rate effect on mechanical properties and fracturing processes is apparent. The influences of the strain rate on various mechanical properties of rocks and other materials, e.g. strength, fracture toughness, elastic modulus, are studied by different laboratory methods such as drop weight test [18, 19], impact test [20, 21], split Hopkinson pressure bar (SHPB) test [22-30], vertical single stage powder gun [31, 32], nano-impact indentation technique [33, 34], true triaxial SHPB test [35, 36] and laboratory or in-situ blasting[37]. The strain rate ranges generated by these test method are illustrated in **Figure 1**. The previous studies indicate that the tensile and compressive strength [23, 38, 39], the shear strength [40], the elastic modulus[38, 41, 42], the Poisson's ratio [43] and the three modes of fracture toughness [44, 45] of rocks or rock-like materials all show more or less rate-dependent (generally increases with the strain rate). The influence of strain rate on cracking behaviour is discussed by observing and describing the failure processes of some simplified and ideal specimens [10, 11, 44-48]. However, the mechanism and theory behind the experimental phenomena are seldom discussed in detail, especially in the universal connections between the rate-dependent mechanical properties and the fracturing behaviour. Since there are systematic investigations on the fracturing process of the single-flawed

specimens under quasi-static loadings in material sciences and rock mechanics, and the analytical solution of the stress around an elliptical flaw has been given in the literature [49], the single-flawed specimens are still used in the dynamic research.

Therefore, the present study tries to determine the connection and interactions between rate-dependent cracking behaviours and the rate-dependent mechanical properties of rocks through single-flawed marble specimens. The two most significant characters are (1) the higher increase rate of tensile strength with strain rate than compressive strength and (2) the suppression of the tensile cracks under dynamic loadings. By using the micro-element analysis method, we build a bridge between the macroscopic strength and cracks, which can effectively interpret the rate-dependent cracking behaviour or the transition of failure mode through the strain-rate dependent material properties and the analytical stress distribution. The present study proposes two new concepts, "localized strain rate effect" and "transition strain rate". The different increase rates between compressive and tensile strength play a key role. It can provide an insight into the fracturing process under high strain rates.

2 Experimental observations

2.1 Material and specimen

The present test specimens are fabricated from Carrara marble having the advantage of assuming isotropic and homogeneous material. The external loading ranges from quasi-static to dynamic regimes. In addition, fracturing processes of the marble are studied by prismatic specimens containing a pre-existing open flaw with a length of 5mm and aperture of 1mm. The Details about material, specimen and experimental setup are presented in the supplementary material.

The variation of flaw size and inclination angle of the single-flawed specimen can make the research on the complexity more controllable and mathematical. The validity of the theoretical model to explain the transition of failure mode under different strain rates can be estimated and its potential application in more complicated models. The goals of using specimen containing a pre-existing flaw in the present study can be concluded as: (1) physically simulating the natural voids or week zones in rocks; (2) generate a non-homogeneous stress field in a specimen to analyze the influence of dynamic loadings; (3) verify the feasibility of the theoretical model to interpret the different cracking behaviours under various strain rates; (4) estimate the potential of the theoretical model to be applied into more complicated geological conditions.

2.2 Dynamic increase factor of compressive and tensile strength

The dynamic increase factor (DIF), which is the ratio of the dynamic strength and the average quasi-static strength, quantifies the increment of the mechanical strength properties with strain rate. The DIFs for tensile and compressive strength are named TDIF and CDIF, respectively. As shown in **Figure 2**A, both the CDIF and TDIF of the Carrara marble increase rapidly in the dynamic regime with the strain rate as a logarithm relationship, while the values in the quasi-static regime remain almost constant. The average value of the quasi-static compressive strength is 90 MPa, and the quasi-static tensile strength is 6.86 MPa obtained by tests. It is found that the TDIF increases much faster than the CDIF in the dynamic regime, which indicates that the tensile strength is more sensitive to the strain rate for Carrara marble and other brittle materials. The fitting curves of Carrara marble are also shown in **Figure 2**A. Most of the DIF-strain rate relationship can be described by a semi-log equation [21, 50, 51]. Since there is a gap of strain rates from 10^{-3} to 1 s^{-1} for the Carrara marble, we follow a similar

practice in the previous studies [52] by fitting two straight lines to cover this range. Because of a faster increase of tensile strength, when the dynamic strain rate increases to a particular value, the dynamic tensile strength can be equal to (like metal) or even higher than the compressive strength, which will be the most essential point in the present study.

$$CDIF = 1.426 + 1.390\,log\,\dot{\varepsilon} \qquad for\ 0.5\ s^{-1} \le \dot{\varepsilon} \le 600\ s^{-1} \qquad \textbf{Eq. 1}$$

$$CDIF = 1 \qquad for\ \dot{\varepsilon} < 0.5\ s^{-1}$$

$$TDIF = 2.414 + 3.784\,log\,\dot{\varepsilon} \qquad for\ 0.5\ s^{-1} \le \dot{\varepsilon} \le 600\ s^{-1} \qquad \textbf{Eq. 2}$$

$$TDIF = 1.229 + 0.043\,log\,\dot{\varepsilon} \qquad for\ \dot{\varepsilon} < 0.5\ s^{-1}$$

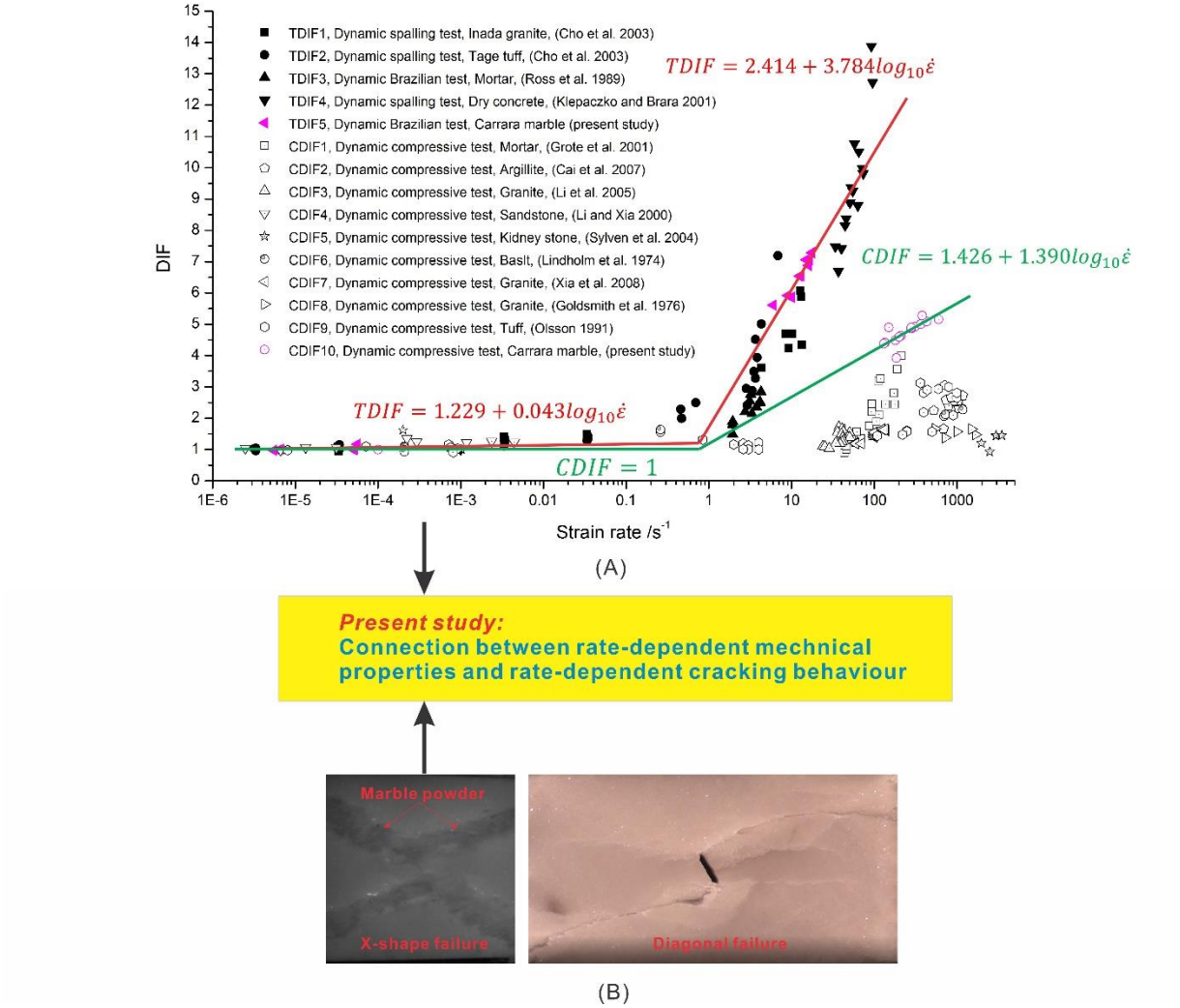

Figure 2. (A) Compressive DIFs and tensile DIFs of different brittle materials and (B) the different cracking and failure modes under quasi-static and dynamic loadings [26, 53-65]. The pink data points are obtained in the present study.

2.3 Fracturing processes of single-flawed marble

The crack initiation and propagation of single-flawed rocks under quasi-static loadings have been comprehensively studied [49, 66-72]. But there are relatively fewer studies in the dynamic regime [73, 74]. The fracturing processes of marble generally can be divided into two stages: white patch development and macro-crack development[11]. It was reported that the influence of loading rate on the white patch development at the early stage of loading is very limited[11].

The failure modes under quasi-static and dynamic loadings are wholly different. Under quasi-static loadings, the fracturing process follows the nucleation-propagation model like other brittle material, as shown in **Figure 2**B. A pair of tensile crack initiates first symmetrically around the pre-set flaw. With the increase of the external load, another pair of cracks with the mixed tensile-shear type initiates and replaces the first pair and leads to specimen failure. In contrast, under dynamic loadings, two pairs of patterns formed by material crushing constitute the fracturing process. Marble powder spatter is universally observed in the cracking process under dynamic loadings (**Figure 2**B) and indicates the fast compression induced volumetric failure. The progressive deformation leads the shear failure without the observation of typical tensile failure. These two pairs of "X" shaped failure patterns, also can be called "macro-cracks", dominate the failure mode. The most significant phenomenon under dynamic failure is the suppression of the tensile cracks under dynamic loadings indicating volumetric failure under shear deformation caused by compressive force.

3. Analytical solution of tangential stress around an elliptical flaw

The analytical solution of the stress around an elliptical flaw is given by **Eq. 3**, while the normal stress along the flaw boundary is zero. Please find the details in the supplementary material, including the assumptions of the solution and the error magnitude. The coordinate and flaw system are shown in **Figure 3**.

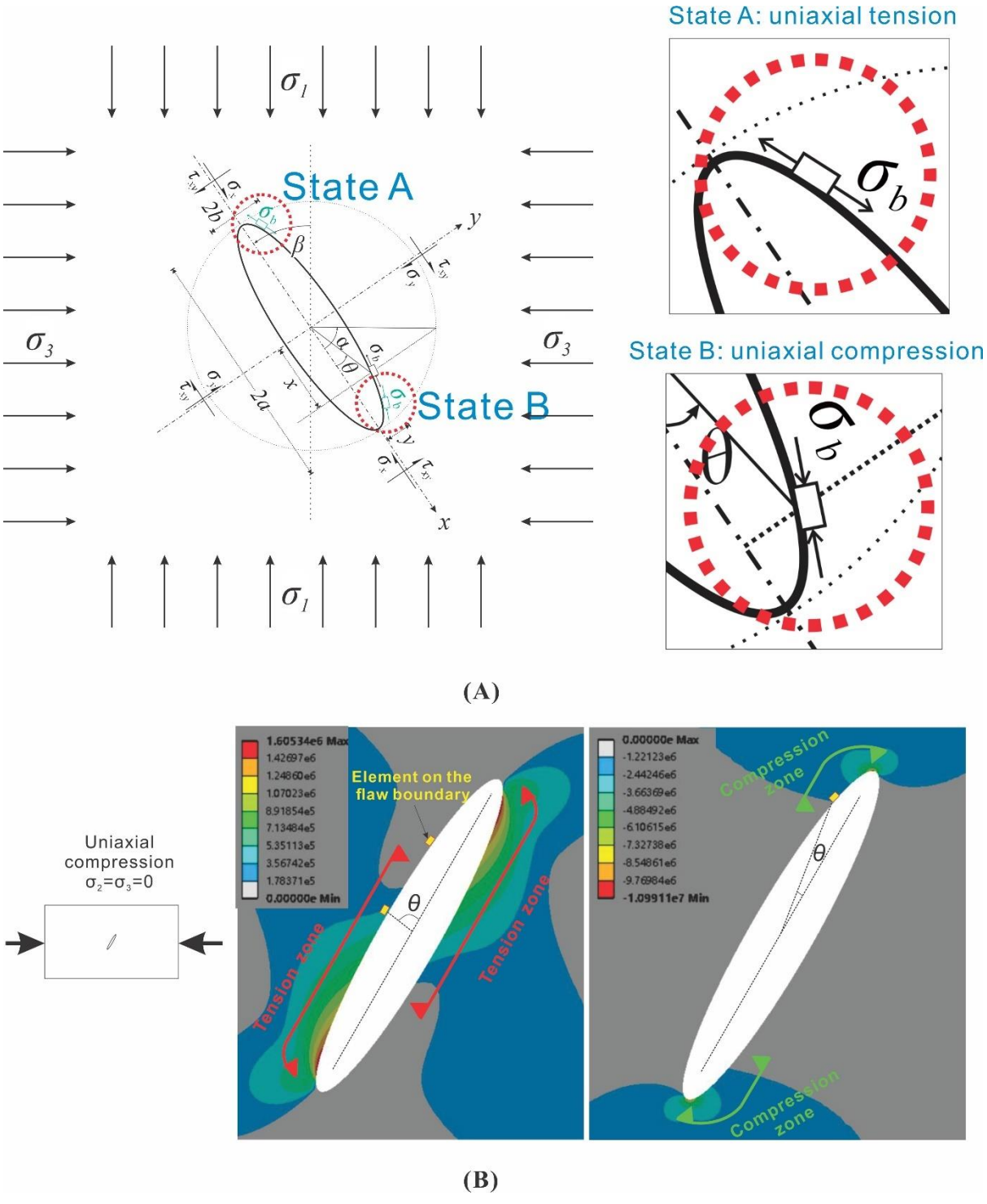

Figure 3. Stress system acting on an elliptical open flaw. (A) Micro-element and stress state along the flaw boundary and (B) tangential stress distribution and the element along the ellipse boundary. The inclination angle between the major axis of the ellipse and the vertical axis is 30° ($\beta = 60°\ and\ m = 1/6$)

$$\sigma_b = \frac{1}{m^2 cos^2\alpha + sin^2\alpha}\Big\{\sigma_y\{m(m+2)cos^2\alpha - sin^2\alpha\} + \sigma_x\{(1+2m)sin^2\alpha - m^2 cos^2\alpha\} - \tau_{xy}\{2(1+m^2)\sin\alpha\cos\alpha\}\Big\} \quad \textbf{Eq. 3}$$

where α is the eccentric angle; $m = b/a$ is the ratio of the minor to the major axis; β is the angle between the loading direction of σ_1 and the long axis of the elliptical flaw; σ_b is the tangential stress on the ellipse boundary. For brittle materials like rock, the coefficient *m* can be assumed as very small.

For the micro-element along the flaw boundary, as shown in **Figure 3**A, since the stress normal to the ellipse boundary is zero, the elements along the ellipse can be seen as a one-dimensional stress state in the 2D simulation. The tangential direction is also the direction of the principal stress. Some elements experience a uniaxial tension state (σ_b < 0) denoted by σ_{bt}, while others experience uniaxial compression state (σ_b > 0) denoted by σ_{bc}. The failure of the micro-element is determined by comparing the stress state and the corresponding strength: (A) if $|\sigma_{bmin}| \geq |\sigma_{bt}|$ and $\sigma_{bmax} < \sigma_{bc}$, the element fails as a tensile mode; (B) otherwise, if the $|\sigma_{bmin}| < |\sigma_{bt}|$ and $\sigma_{bmax} \geq \sigma_{bc}$, the element fails as a compressive/shear mode.

The analytical solution can be verified by the numerical method - finite element method[75]. **Figure 3**B illustrates the contour of the principal stress around the flaw with an inclination angle of 30° given by numerical simulation. The tension zone and the compression zone matches the analytical solution well, according to the figure.

4. Crack initiation mode and corresponding tangential stress considering strain rate effect

The present section devotes the rate-dependence of strength to the rate-dependence of failure mode and the determination of the transition strain rate. From the perspective of strength, crack initiates when either the tensile or the compressive stress reaches the corresponding strength of a micro-element. The fast stress redistribution then makes a progressive failure of micro-elements and forms the macroscopic cracks.

The failure behaviour under tension and compression stresses shows a significant difference in the fracturing process. Compression failure can produce violent crushing and a larger angle between the first principal stress and the crack pattern. The compression failure usually behaves in a shear crack pattern. In section 2, dynamic loading shows more compression failure than tension failure. The latter generally dominates the quasi-static loading condition. The result indicates that the anti-tension strength increases significantly compared with the anti-compression strength, consistent with the above experimental observation about strength. In other words, it is the different rate-dependence between tensile and compressive strength affecting the cracking behaviour and failure mode.

It is essential to point out that the strain rate of virtual micro-elements inside the specimen is not even due to the stress concentration effect around the crack tip or defects. This concept is different from previous studies on rock dynamics, in which the strain rate of all the micro-elements inside a specimen is thougt to be even and equal the applied strain rate on the specimen ends. Due to the uneven strain distribution, the strain rate is also uneven inside the specimen because the strain variation rate is proportional to the stress variation rate in the elastic stage. Consequently, the strain rate of elements around the flaw is typically higher than other parts contributed by the high stress or strain concentration.

4.1 Strain rate dependent strength

Since the strain rate influences the mechanical properties, uneven strain rate distribution for a nonintact specimen can induce uneven mechanical properties. We refer to this phenomenon as "***localized mechanical properties***". Among many mechanical properties, the influence on rock strength by the strain rate is most apparent and can be quantitatively evaluated/characterized. The "***localized strength***" varies with the applied strain rate on the specimen by external dynamic loadings. Due to higher increase rate of dynamic tensile strength, under a very high strain rate, the tensile strength of an element around a flaw might keep larger than the principal tensile stress when the compressive strength is equal or lower than the principal compressive stress. This fact can alter the cracking behaviour of a nonintact specimen, which we nominate as "***localized strain rate effect***" in the present study. This effect can be neglected under quasi-static loading conditions due to the extremely low strain rate and its insensitivity to strain rate but should be considered under high-rate loadings.

We first investigate the localized strain rate effect on the mechanical properties and the crack initiation in a nonintact specimen. The region around the flaw is divided into many virtual micro-elements to describe the localized strain rate and strength. If the strain is tensile, the strain rate is negative. Otherwise, it is positive. Element strain rate $\dot{\varepsilon}_{pb}$, which is defined by the strain rate of a micro-element around the flaw, can be calculated by dividing the variation rate of the element stress by the material elastic modulus, as shown in **Eq. 4**. According to many previous studies [76], the elastic modulus is not very sensitive to strain rate. To simplify the analytical model, it is assumed that change of the elastic modulus can be neglected in such a strain rate range. The elementary strain rate around the flaw $\dot{\varepsilon}_{pb}$ is given by **Eq. 4**.

$$\dot{\varepsilon}_{pb} = \frac{\dot{\sigma_b}}{E} = \frac{\dot{\sigma_b}}{\dot{\sigma_1}} \cdot \frac{\dot{\sigma_1}}{E} = \frac{\dot{\sigma_b}}{\dot{\sigma_1}} \dot{\varepsilon_1} \qquad \textbf{Eq. 4}$$

The strain rate dependence on the uniaxial compressive and tensile strength is usually regarded as the common logarithm of strain rate [77], which has the form of the following equations:

$$CDIF = A_c + B_c \, lg \, \dot{\varepsilon}_{pb} \qquad in\ dynamic\ regime\ m_c \le \dot{\varepsilon}_{pb} \le n_c$$

$$CDIF = C_c + D_c \, lg \, \dot{\varepsilon}_{pb} \qquad in\ quasi-static\ regime\ \ \dot{\varepsilon}_{pb} < m_c \qquad \textbf{Eq. 5}$$

$$TDIF = A_t + B_t \, lg \, \dot{\varepsilon}_{pb} \qquad in\ dynamic\ regime\ m_t \le \dot{\varepsilon}_{pb} \le n_t$$

$$TDIF = C_t + D_t \, lg \, \dot{\varepsilon}_{pb} \qquad in\ quasi-staci\ regime\ \dot{\varepsilon}_{pb} < m_t \qquad \textbf{Eq. 6}$$

where A_c, B_c, C_c, D_c, A_t, B_t, C_t and D_t are the coefficients for the compressive and tensile DIFs, respectively; m_c, n_c, m_t and n_t are the lower and upper limits for the compressive and tensile strain rate regimes, respectively.

Then, the dynamic tensile strength σ_{dt} and the dynamic compressive strength σ_{dc} under a certain strain rate can be given by

$$\sigma_{dt} = TDIF \cdot \sigma_t = (A_t + B_t \, log|\dot{\varepsilon}_{pb}|) \cdot \sigma_t \text{ , for } m_t \le |\dot{\varepsilon}_{pb}| \le n_t \qquad \textbf{Eq. 7}$$

$$\sigma_{dc} = CDIF \cdot \sigma_c = \left(A_c + B_c \, log \, \dot{\varepsilon}_{pb}\right) \cdot \sigma_c, \text{ for } m_c \le \dot{\varepsilon}_{pb} \le n_c \qquad \textbf{Eq. 8}$$

In the uniaxial compression tests, $\sigma_1 > 0$, $\sigma_3 = 0$, and $\sigma_{13} = 0$, which gives

$$\sigma_x = \frac{\sigma_1}{2} + \frac{\sigma_1}{2} \cdot \cos 2\beta \qquad \textbf{Eq. 9}$$

$$\sigma_y = \frac{\sigma_1}{2} - \frac{\sigma_1}{2} \cdot \cos 2\beta \qquad \textbf{Eq. 10}$$

$$\tau_{xy} = \frac{\sigma_1}{2} \cdot \sin 2\beta \qquad \textbf{Eq. 11}$$

Based on **Eq. 3**, the tangential stress on the boundary of the ellipse σ_b becomes

$$\sigma_b = \frac{\sigma_1}{m^2 cos^2\alpha + sin^2\alpha}\left\{\left(\frac{1}{2} - \frac{1}{2}\cdot\cos 2\beta\right)[m(m+2)cos^2\alpha - sin^2\alpha]\right.$$
$$+ \left(\frac{1}{2} + \frac{1}{2}\cdot\cos 2\beta\right)[(1+2m)sin^2\alpha - m^2 cos^2\alpha]$$
$$\left. - (1+m^2)\sin 2\beta \sin\alpha\cos\alpha\right\} = \mathrm{M}(\alpha,\beta,m)\sigma_1 \qquad \textbf{Eq. 12}$$

Substituting **Eq. 12** into **Eq. 4** gives:

$$\dot{\varepsilon}_{pb} = \frac{\dot{\sigma_b}}{\dot{\sigma_1}}\dot{\varepsilon}_1 = \frac{\dot{\varepsilon_1}}{m^2 cos^2\alpha + sin^2\alpha}\left\{\left(\frac{1}{2} + \frac{1}{2}\cdot\cos 2\beta\right)[m(m+2)cos^2\alpha - sin^2\alpha]\right.$$
$$+ \left(\frac{1}{2} - \frac{1}{2}\cdot\cos 2\beta\right)[(1+2m)sin^2\alpha - m^2 cos^2\alpha]$$
$$\left. - (1+m^2)\sin 2\beta \sin\alpha\cos\alpha\right\} = \mathrm{M}(\alpha,\beta,m)\dot{\varepsilon}_1 \qquad \textbf{Eq. 13}$$

It is noted that $\dot{\varepsilon}_{pb} > 0$ means the compressive strain rate, while $\dot{\varepsilon}_{pb} < 0$ means the tensile strain rate. To be specific, if the element strain rate is assumed to be $\dot{\varepsilon}_{pb}$, when the principal compressive stress σ_{bc} equals the corresponding dynamic compressive strength σ_{dc} ($\sigma_{bc} \geq \sigma_{dc}$), the compressive failure will occur. Otherwise, when the principal tensile stress σ_{bt} equals the corresponding dynamic tensile strength σ_{dt} ($\sigma_{bt} \leq \sigma_{dt}$), the tensile failure will occur.

4.2 Transition strain rate

Along the flaw boundary, under quasi-static loadings, the tensile strength of a rock is much lower than the compressive strength, which means the tensile failure of the element generally appears first. However, for most of the brittle materials, according to **Figure 2**, the tensile strength increases faster than the compressive strength with the strain rate, which indicates that the failure mode under dynamic loadings is not only tensile, especially when the dynamic strain rate rises to a specific value –***transition strain rate*** $\dot{\varepsilon_{tr}}$. For the single-flawed specimen, the transition strain rate $\dot{\varepsilon_{tr}}$ is defined as the applied strain rate corresponding to the transition of crack type or failure mode from tensile to compressive (shear). When the applied

strain rate on a specimen achieves this transition strain rate, the maximum tangential stress equals the corresponding dynamic compressive strength; meanwhile, the absolute value of the minimum tangential stress equals the corresponding dynamic tensile strength. When the applied strain rate of the specimen is higher than the $\dot{\varepsilon_{tr}}$, the crack type, initiation position, failure mode and propagation of the first cracks will be significantly changed.

For the single-flawed specimen under uniaxial compression ($\sigma_1 > 0$, $\sigma_3 = 0$, and $\sigma_2 = 0$), the transition strain rate $\dot{\varepsilon_{tr}}$ under dynamic loadings is given by the following equation. The deduction can be found in the elementary material.

$$\dot{\varepsilon_{tr}} = \left[\frac{(-\mathrm{M}(\alpha_{min},\beta,m))^{\frac{B_t \mathrm{M}(\alpha_{max},\beta,m)\sigma_t}{-\mathrm{M}(\alpha_{min},\beta,m)\sigma_c}} \times 10^{\frac{A_t \mathrm{M}(\alpha_{max},\beta,m)\sigma_t}{-\mathrm{M}(\alpha_{min},\beta,m)\sigma_c} - A_c}}{\mathrm{M}(\alpha_{max},\beta,m)^{B_c}}\right]^{\frac{1}{B_c - \frac{B_t \mathrm{M}(\alpha_{max},\beta,m)\sigma_t}{-\mathrm{M}(\alpha_{min},\beta,m)\sigma_c}}}$$

Eq. 14

4.3 Transition strain rate of a single-flawed specimen with 30° inclination angle

In this section, the transition strain rate of a single-flawed specimen is analyzed. The specimen containing an elliptical flaw with a 30° inclination angle ($\beta = 60°\ and\ m = 1/6$) are investigated under uniaxial compression. First, the maximum tensile and compressive tangential stress should be determined as well as their positions around the flaw. When the geometry of the specimen is confirmed, the tangential stress σ_b depends on both the uniaxial compression stress σ_1 and the eccentric angle α along the elliptical flaw boundary. According to the analytical solution, the variation of σ_b regarding the eccentric angle α under uniaxial compression stress σ_1 is illustrated in **Figure 4**. The normalized tangential stress is defined as the ratio of σ_b and σ_1. There are two local extrema for the normalized tangential stress. One represents the maximum tensile stress and marks as σ_{bmin} with the corresponding eccentric angle α_{min}. The other one represents the maximum compressive stress and marks as σ_{bmax}

with the corresponding eccentric angle α_{max}. From **Eq. 12**, the normalized tangential stress equals the function $\mathrm{M}(\alpha, \beta, m)$.

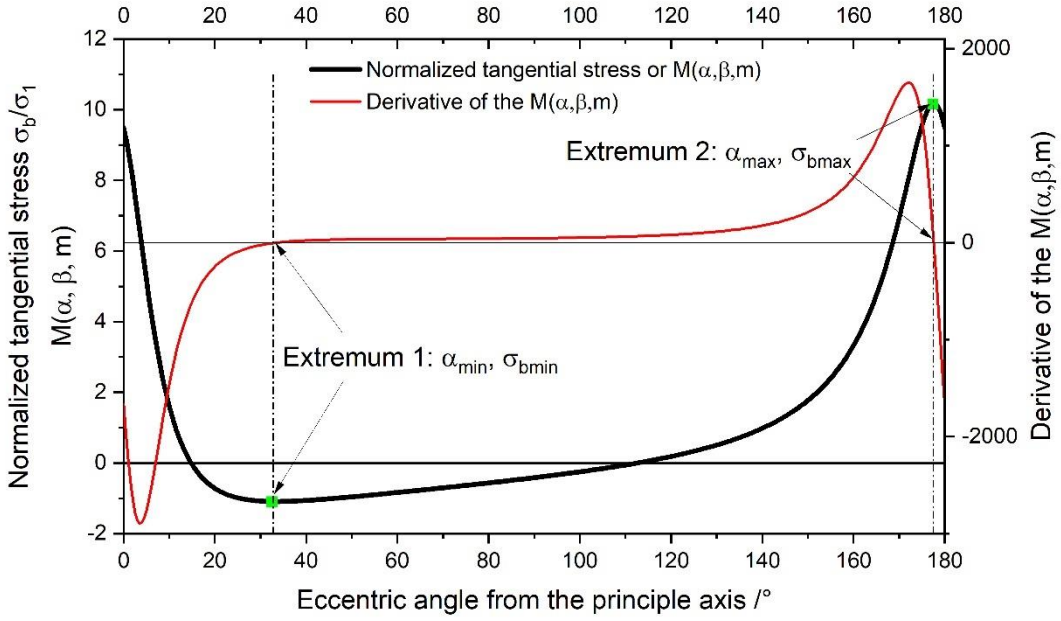

Figure 4. Normalized tangential stress along the elliptical flaw boundary regarding the eccentric angle from the principal axis for the single-flawed specimen with the inclination angle of 30°

The eccentric angles α_{min} and α_{max} corresponding to the the minimum stress σ_{bmin} (maximum tensile stress) and the maximum compressive stress σ_{bmax} can be determined by the derivative of the $\mathrm{M}(\alpha, \beta, m)$.

$$\frac{\partial \mathrm{M}(\alpha, \beta, m)}{\partial \alpha} = \frac{\partial \mathrm{M}(\alpha, 60, 1/6)}{\partial \alpha} = 0 \qquad \textbf{Eq. 15}$$

where α varies from 0 to 180°. The solutions of the eccentric angles α_{min} and α_{max} are 33.5° and 177.6°, while the corresponding values of the $\mathrm{M}(\alpha_{min}, \beta, m)$ and $\mathrm{M}(\alpha_{max}, \beta, m)$ are determined to be -1.09 and 10.17, respectively. Details about the solution can be found in the supplementary material.

Therefore, based on **Eq. 14**, the $\dot{\varepsilon_{tr}}$ can be derived as

$$\dot{\varepsilon_{tr}} = \left(\frac{2.24^{Bt\cdot\frac{\sigma_t}{\sigma_c}} \times 10^{9.33At\cdot\frac{\sigma_t}{\sigma_c}-Ac}}{10.17^{Bc}}\right)^{1/(Bc-9.33Bt\cdot\frac{\sigma_t}{\sigma_c})} \quad \textbf{Eq. 16}$$

For Carrara marble, according to the laboratory result shown in **Eq. 1** and **Eq. 2**, the coefficients A_c, B_c, A_t, and B_t for the marble are determined to be 1.426, 1.390, 2.414 and 3.784 ($0.5\ s^{-1} \leq \left|\dot{\varepsilon}_{pb}\right|$ for both compressive and tensile strain rate). Therefore, the transition strain rate, for the single-flawed marble specimen with 30° inclination angle, is calculated to be 5.95 s^{-1} according to **Eq. 16**. When the applied strain rate is higher than the transition strain rate $\dot{\varepsilon_{tr}} \geq \dot{\varepsilon_1}$, the compressive/shear failure will occur first associating the shear crack; otherwise, the tensile failure will occur first associating the tensile crack.

4.4 Importance of rate-dependent strength and localized strain rate effect

Three cases are used to evaluate the importance of considering the localized strain rate effect in analysing dynamic cracking behaviour. The analysis model is also a marble specimen containing a single flaw inclined at 30° with the applied strain rate of 150 s^{-1} on the loading surface. The first case considers none of the rate-dependent strength and the localized strain rate effect. The second case only considers the uneven stress distribution and the rate-dependent strength for the average applied strain rate. In contrast, the third case considers the localized strain rate effect, which means the strain rate distribution inside the specimens is uneven. The result shows that the dynamic failure mode is similar to the quasi-static condition without considering the localised strain rate effect. Thus, the localized strain rate effect on strength is the key to explain the different cracking behaviours under dynamic loadings.

4.4.1 Case without considering rate-dependent strength and localized strain rate effect

This case is the mechanical analysis under quasi-static loading condition. According to the previous analysis, the tangential stress along the elliptical flaw boundary is shown in **Figure**

5A. If the rate-dependent strength and the localized strain rate effect are both not considered, the strength is constant and equals the quasi-static value. Since the tensile strength is much lower than the compressive strength, tensile failure always occurs first. This case study indicates that in high strain rate loading, the influence of strain rate on strength must be considered.

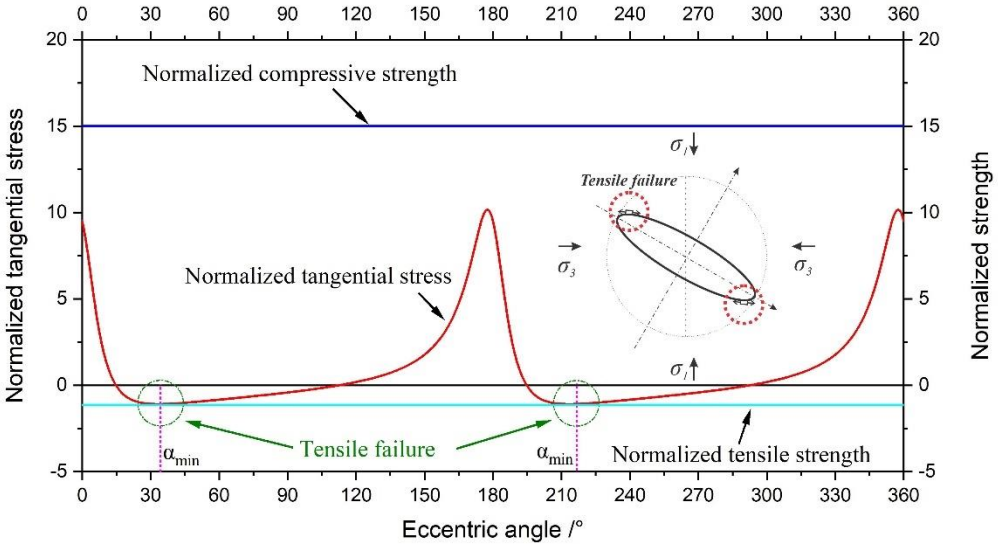
Normalized compressive strength
Normalized tangential stress
Tensile failure
Normalized tensile strength
α_{min}
α_{min}
Normalized tangential stress
Normalized strength
Eccentric angle /°

（A）

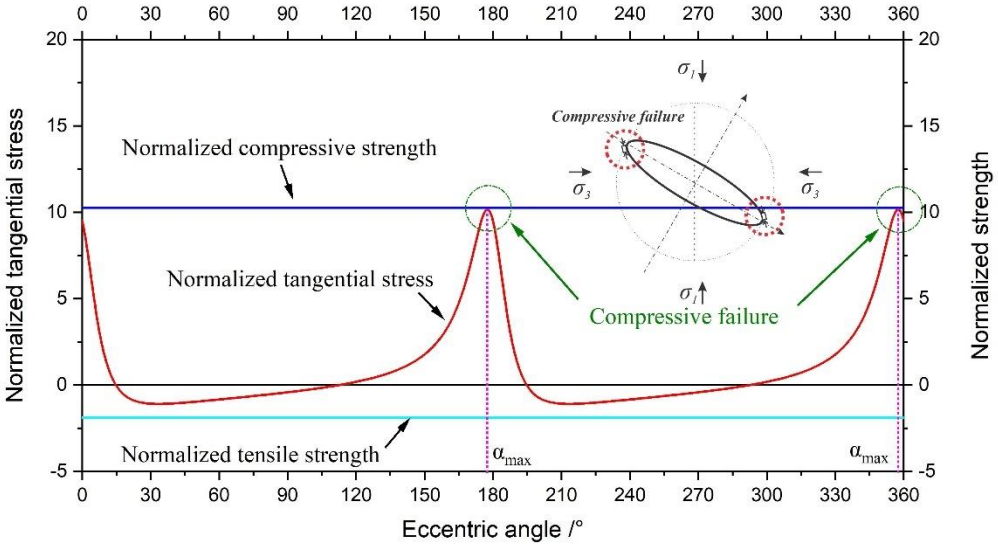
Normalized compressive strength
Normalized tangential stress
Compressive failure
Normalized tensile strength
α_{max}
α_{max}
Normalized tangential stress
Normalized strength
Eccentric angle /°

（B）

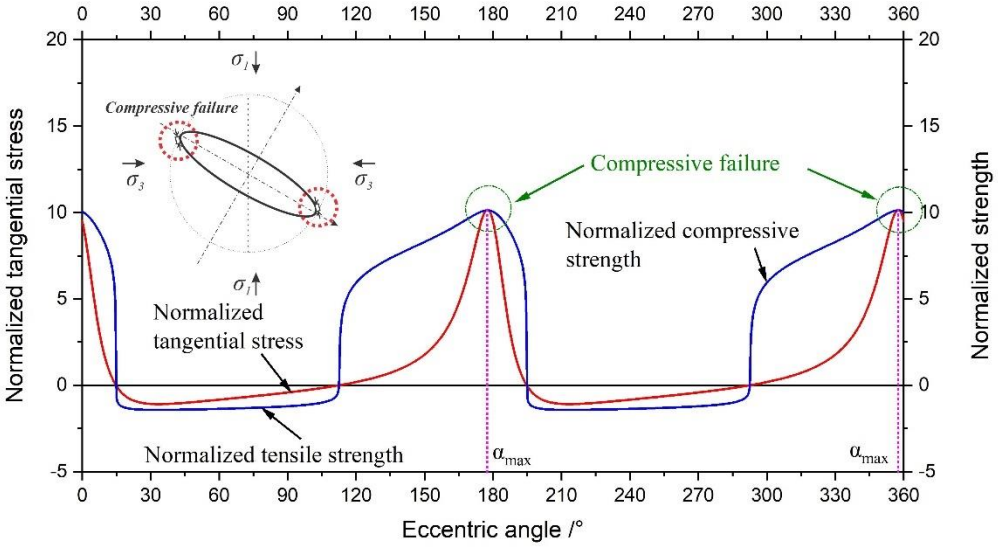
Compressive failure
Normalized tangential stress
Normalized compressive strength
Normalized tensile strength
α_{max}
α_{max}
Normalized tangential stress
Normalized strength
Eccentric angle /°

（C）

Figure 5. Tangential stress along the elliptical flaw boundary and the corresponding strength of the single-flawed specimen with the inclination angle of 30° tested (A) under the strain rate of 0.01 s^{-1} without considering the strain rate effect; (B) under the strain rate of 150 s^{-1} without considering the strain rate effect; (C) under the strain rate of 150 s^{-1} considering both the strain rate effect and the localized strain rate effect.

4.4.2 Case without considering localized strain rate effect

This case is the mechanical analysis under dynamic loading (strain rate 150 s^{-1}) condition. The strength is not considered rate-dependent; however, it is constant because the localized strain rate effect is not considered. In this case, though the tangential stress at failure along the elliptical flaw boundary increases significantly, the normalized tangential stress is still identical (**Figure 5**B). The failure mode changes from tensile failure to compressive failure. Though the dynamic tensile strength is much lower than the compressive strength, the maximum tensile tangential stress is lower than the tensile strength. Thus, tensile failure is suppressed due to the faster dynamic increase of tensile strength than compressive strength. This case study indicates that in high strain rate loading, the influence of strain rate on strength must be considered.

4.4.3 Case considering localized strain rate effect

This case analyzes the variation of tangential stress and strength under dynamic loading (strain rate 150 s^{-1}) condition. Both the rate-dependent strength and the localized strain rate effect are considered. Similar to the previous case, the normalized tangential stress is still identical to **Figure 5**A and **Figure 5**B. Due to the variation of the localized strain rate along the flaw boundary, the element strength changes around the flaw because of the rate-dependence strength shown in **Figure 5**C. The compressive and the tensile strength are then normalized by being divided by the uniaxial stress σ_1. The normalized tangential stress obtained from the

equations is compared with the normalized strength for various eccentric angles from 0 to 360°. As a result, we can find that rock material failure will first occur under maximum dynamic compressive stress rather than tensile failure under quasi-static loading. Here, the transition strain rate is defined as the one under which the maximum and minimum normalized tangential stresses are simultaneously equal to the normalized compressive and the tensile strength, respectively. If a crack initiates at this place, the style of this crack is shear. The powders and micro-cracks associating the cracking process also indicates the compressive or shear failure. Compared with the quasi-static test, the dynamic crack initiation point and the crack type are all changed.

According to the result, the strain rate hardening on the tensile strength is more prominent, and the development of tensile failure might be suppressed compared with that of compressive failure. This finding is proposed to be the leading cause of the different cracking behaviours under quasi-static and dynamic conditions. The suppression of the tensile crack can be well explained by this model. The tensile crack may not be the first crack in the dynamic loading case. Thus, the tensile failure assumption, typically prevalent in quasi-static analytical solutions, will face a significant challenge under dynamic loadings.

5 Discussion and conclusion

5.1 Discussion

In the theoretical analysis, the flaw is a perfect ellipse. However, the flaw tip in the experimental study is round due to the limitation of the fabrication technique. Whether such a difference in the flaw shape can affect the previous findings should be studied. The numerical simulation reveals that the slight difference between the experimental and theoretical flaw shape only has a minor influence on the regularity of the transition strain rate.

According to the present study, the rapid increase of tensile strength, preventing the development of tensile cracks. However, under dynamic loadings, the two groups of symmetrical “X” shaped cracks at the boundary of the pre-existing flaw initiate nearly simultaneously and forms the failure. One plausible interpretation is that though the normalized tangential stress reaches the normalized compressive strength first, the negative normalized tangential stress is also very close to the normalized tensile strength (**Figure 5**). Another plausible interpretation is that the plasticity of marble is higher than that of other brittle rocks under dynamic loadings, which is evident by white patches and the increase of failure strain under dynamic loadings. The plasticity can allow rapid stress redistribution and decrease the stress concentration. The consequence is the slowdown of crack development, and further load can still be sustained after the initiation of the first cracks.

The present study uses the single-flawed specimen to investigate the dynamic cracking process. The influence of the neighbouring flaws or defects is not considered. However, the research result on the double-flawed specimens indicates that the X-shape failure mode is still the dominant mode for double-flawed specimens. The proposed explanation for the suppression of the tensile cracks is universal as long as the tensile strength of the material is more sensitive to the strain rate than the compressive strength under dynamic loadings, according to Eq. 16. The suppression of tensile cracks will happen when the strain rate applied on the specimen is higher than the transition strain rate. The only difference is the value of the transition strain rate for different materials.

More details about the previous discussions can be found in the supplementary material.

5.2 Conclusions

This paper explains why tensile cracks are suppressed and shear crack bands dominate the failure of rock containing flaws under rapid loadings. Uneven distribution of strain rate

around the flaw and different rate-dependencies of tensile and compressive strength are the crucial points of the present research. By using the micro-element analysis method, the concepts of the “localized strain rate effect” is proposed and believed to lead to the variation of cracking behaviours under different loading rates. The “transition strain rate” concept, which contains four variants, including the strain rate, rate-dependent tensile strengths, rate-dependent compressive strengths and flaw geometry, is derived as a watershed for the different cracking behaviours.

The key findings of the present paper include:

(1) The tensile strength of marble is more sensitive to the strain rate reflected by the significantly higher tensile dynamic increase factor (DIF) compared with the compressive DIF.

(2) The strain rate field around the flaw is not even. The "localized strain rate effect" enhance the different dynamic tensile and compressive strength.

(3) Due to the localized strain rate effect, the faster increase of tensile strength will be larger than the maximum dynamic tensile stress when the strain rate is higher than the "transition strain rate", resulting in the suppression of tensile cracks or failure.

Acknowledgements

The experimental data presented in this paper is obtained from the lab tests conducted by the authors in the Construction and Testing Laboratory at Nanyang Technological University. The first author appreciates the supervision and guidance of Louis Ngai Yuen Wong and the assistance of Weng Kong Cheng in the SHPB tests. The authors are also grateful for the inspiring discussion with the group members at Monash University. This work was supported by the National Natural Science Foundation of China (No. 41525009, 41831281).

Reference

1. Ma G, Hao H, Wang F. Simulations of explosion-induced damage to underground rock chambers. *J Rock Mech Geotech Eng.* 2011;3(1): 19-29.
2. Turcotte DL. Fractals and fragmentation. *Journal of Geophysical Research: Solid Earth.* 1986;91(B2): 1921-1926.
3. Melosh HJ, Ryan EV, Asphaug E. Dynamic fragmentation in impacts: Hydrocode simulation of laboratory impacts. *Journal of Geophysical Research: Planets.* 1992;97(E9): 14735-14759.
4. Goldsby DL, Tullis TE. Flash heating leads to low frictional strength of crustal rocks at earthquake slip rates. *Science.* 2011;334(6053): 216-218.
5. Mishra S, Khetwal A, Chakraborty T. Dynamic characterisation of gneiss. *Rock Mechanics and Rock Engineering.* 2019;52(1): 61-81.
6. Levitas VI, Ravelo R. Virtual melting as a new mechanism of stress relaxation under high strain rate loading. *Proceedings of the National Academy of Sciences of the United States of America.* 2012;109(33): 13204.
7. Fredrich JT, Evans B, Wong T-F. Micromechanics of the brittle to plastic transition in Carrara marble. *Journal of Geophysical Research: Solid Earth.* 1989;94(B4): 4129-4145.
8. Grady DE, Kipp ME. Dynamic rock fragmentation. In: Atkinson BK, ed. *Fracture Mechanics of Rock.* London: Academic Press; 1987:429-475.
9. Meyers MA. *Dynamic behavior of materials / Marc A. Meyers*: New York ; Singapore : John Wiley & Sons, Inc., 1994.; 1994.
10. Zou C, Wong LNY, Loo JJ, Gan BS. Different mechanical and cracking behaviors of single-flawed brittle gypsum specimens under dynamic and quasi-static loadings. *Eng Geol.* 2016;201: 71-84.
11. Zou C, Wong LNY. Experimental studies on cracking processes and failure in marble under dynamic loading. *Eng Geol.* 2014;173(0): 19-31.
12. Kalthoff J. Shadow optical analysis of dynamic shear fracture. *Opt Eng.* 1988;27(10): 271035.
13. Ravi-Chandar K, Lu J, Yang B, Zhu Z. Failure mode transitions in polymers under high strain rate loading. *Int J Fract.* 2000;101(1-2): 33-72.
14. Sokovikov M, Simonov M, Bilalov D, et al. Mechanical and microstructural aspects of material failure due to localized shear under high-rate loading conditions. *AIP Conf Proc.* 2018;2051(1): 020292.
15. Zhou M, Rosakis AJ, Ravichandran G. Dynamically propagating shear bands in impact-loaded prenotched plates—I. Experimental investigations of temperature signatures and propagation speed. *Journal of the Mechanics and Physics of Solids.* 1996;44(6): 981-1006.
16. French BM, McKay RM, Liu HP, Briggs DEG, Witzke BJ. The Decorah structure, northeastern Iowa: Geology and evidence for formation by meteorite impact. *GSA Bulletin.* 2018;130(11-12): 2062-2086.
17. Kalthoff JF. Modes of dynamic shear failure in solids. *Int J Fract.* 2000;101(1): 1-31.
18. Bearman R, Briggs C, Kojovic T. The applications of rock mechanics parameters to the prediction of comminution behaviour. *Miner Eng.* 1997;10(3): 255-264.
19. Banthia N, Mindess S, Bentur A, Pigeon M. Impact testing of concrete using a drop-weight impact machine. *Exp Mech.* 1989;29(1): 63-69.
20. Grady DE, Kipp ME. The micromechanics of impact fracture of rock. *International Journal of Rock Mechanics and Mining Sciences & Geomechanics Abstracts.* 1979;16(5): 293-302.
21. Zhao J, Zhou YX, Hefny AM, et al. Rock dynamics research related to cavern development for ammunition storage. *Tunnelling Underground Space Technol.* 1999;14(4): 513-526.
22. Davies EDH, Hunter SC. The dynamic compression testing of solids by the method of the split Hopkinson pressure bar. *Journal of the Mechanics and Physics of Solids.* 1963;11(3): 155-179.
23. Frew D, Forrestal M, Chen W. A split Hopkinson pressure bar technique to determine compressive stress-strain data for rock materials. *Exp Mech.* 2001;41(1): 40-46.
24. Lok TS, Li XB, Liu D, Zhao PJ. Testing and response of large diameter brittle materials subjected to high strain rate. *J Mater Civ Eng.* 2002;14(3): 262-269.
25. Dai F, Xia K, Zheng H, Wang YX. Determination of dynamic rock Mode-I fracture parameters using cracked chevron notched semi-circular bend specimen. *Eng Fract Mech.* 2011;78(15): 2633-2644.

26. Li XB, Lok TS, Zhao J. Dynamic Characteristics of Granite Subjected to Intermediate Loading Rate. *Rock Mech Rock Eng.* 2005;38(1): 21-39.
27. Kandula N, Cordonnier B, Boller E, Weiss J, Dysthe DK, Renard F. Dynamics of microscale precursors during brittle compressive failure in Carrara marble. *Journal of Geophysical Research: Solid Earth.* 2019;124(6): 6121-6139.
28. Li D, Han W, Jiang L. High strain rate impact effect and failure behavior of 3D six-directional braided composites. *Extreme Mech Lett.* 2021;45: 101291.
29. Li XF, Li HB, Zhang QB, Jiang JL, Zhao J. Dynamic fragmentation of rock material: Characteristic size, fragment distribution and pulverization law. *Eng Fract Mech.* 2018;199: 739-759.
30. Zhu Q, Li D, Wang W. Mechanical behavior and permeability evolution of sandstone with confining pressure after dynamic loading. *Geomechanics and Geophysics for Geo-Energy and Geo-Resources.* 2021;7(3): 81.
31. Kawakami S-I, Mizutani H, Takagi Y, Kato M, Kumazawa M. Impact experiments on ice. *Journal of Geophysical Research: Solid Earth.* 1983;88(B7): 5806-5814.
32. Mizutani H, Kawakami S, Takagi Y, Kato M, Kumazawa M. Cratering experiments in sands and a trial for general scaling law. *Journal of Geophysical Research: Solid Earth.* 1983;88(S02): A835-A845.
33. Wheeler JM, Dean J, Clyne TW. Nano-impact indentation for high strain rate testing: The influence of rebound impacts. *Extreme Mech Lett.* 2019;26: 35-39.
34. Ma Z, Pathegama Gamage R, Zhang C. Application of nanoindentation technology in rocks: a review. *Geomechanics and Geophysics for Geo-Energy and Geo-Resources.* 2020;6(4): 60.
35. Liu K, Zhao J. Progressive damage behaviours of triaxially confined rocks under multiple dynamic loads. *Rock Mech Rock Eng.* 2021;54: 1-32.
36. Liu K, Zhao J, Wu G, Maksimenko A, Haque A, Zhang QB. Dynamic strength and failure modes of sandstone under biaxial compression. *Int J Rock Mech Min Sci.* 2020;128: 104260.
37. Chi LY, Zhang ZX, Aalberg A, Yang J, Li CC. Fracture Processes in Granite Blocks Under Blast Loading. *Rock Mech Rock Eng.* 2019;52(3): 853-868.
38. Wang Q, Li W, Song X. A method for testing dynamic tensile strength and elastic modulus of rock materials using SHPB. *Pure Appl Geophys.* 2006;163(5): 1091-1100.
39. Zhao J, Li H. Experimental determination of dynamic tensile properties of a granite. *Int J Rock Mech Min Sci.* 2000;37(5): 861-866.
40. Barbero M, Barla G, Zaninetti A. Dynamic shear strength of rock joints subjected to impulse loading. *Int J Rock Mech Min Sci.* 1996;33(2): 141-151.
41. Ying P, Zhu Z, Ren L, et al. Deterioration of dynamic fracture characteristics, tensile strength and elastic modulus of tight sandstone under dry-wet cycles. *Theor Appl Fract Mech.* 2020;109: 102698.
42. Davarpanah SM, Ván P, Vásárhelyi B. Investigation of the relationship between dynamic and static deformation moduli of rocks. *Geomechanics and Geophysics for Geo-Energy and Geo-Resources.* 2020;6(1): 29.
43. Xing H, Zhang Q, Braithwaite C, Pan B, Zhao J. High-Speed photography and digital optical measurement techniques for geomaterials: fundamentals and applications. *Rock Mech Rock Eng.* 2017;50(6): 1611-1659.
44. Kalthoff JF, Bürgel A. Influence of loading rate on shear fracture toughness for failure mode transition. *International Journal of Impact Engineering.* 2004;30(8–9): 957-971.
45. Zhang QB, Zhao J. Effect of loading rate on fracture toughness and failure micromechanisms in marble. *Eng Fract Mech.* 2013;102(0): 288-309.
46. Li D, Han Z, Sun X, Zhou T, Li X. Dynamic mechanical properties and fracturing behavior of marble specimens containing single and double flaws in shpb tests. *Rock Mech Rock Eng.* 2019;52(6): 1623-1643.
47. Liao Z, Tang C, Yang W, Zhu J. Three-dimensional numerical investigation of rock plate cracking and failure under impact loading. *Geomechanics and Geophysics for Geo-Energy and Geo-Resources.* 2021;7(2): 33.
48. Wang F, Cao P, Zhou C-t, Li C-b, Qiu J-d, Liu Z-z. Dynamic compression mechanical behavior and damage model of singly-jointed samples. *Geomechanics and Geophysics for Geo-Energy and Geo-Resources.* 2020;6(4): 71.

49. Hoek E, Bieniawski ZT. Brittle fracture propagation in rock under compression. *Int J Fract.* 1984;26(4): 276-294.
50. Wasantha PLP, Ranjith PG, Zhao J, Shao SS, Permata G. Strain rate effect on the mechanical behaviour of sandstones with different grain sizes. *Rock Mech Rock Eng.* 2015;48(5): 1883-1895.
51. Li HB, Zhao J, Li TJ. Triaxial compression tests on a granite at different strain rates and confining pressures. *Int J Rock Mech Min Sci.* 1999;36(8): 1057-1063.
52. Hao Y, Hao H. Numerical evaluation of the influence of aggregates on concrete compressive strength at high strain rate. *International Journal of Protective Structures.* 2011;2(2): 177-206.
53. Cho SH, Ogata Y, Kaneko K. Strain-rate dependency of the dynamic tensile strength of rock. *Int J Rock Mech Min Sci.* 2003;40(5): 763-777.
54. Ross CA, Thompson PY, Tedesco JW. Split-Hopkinson pressure-bar tests on concrete and mortar in tension and compression. *ACI Mater J.* 1989;86(5): 475-481.
55. Klepaczko JR, Brara A. An experimental method for dynamic tensile testing of concrete by spalling. *International Journal of Impact Engineering.* 2001;25(4): 387-409.
56. Grote DL, Park SW, Zhou M. Dynamic behavior of concrete at high strain rates and pressures: I. experimental characterization. *International Journal of Impact Engineering.* 2001;25(9): 869-886.
57. Cai M, Kaiser P, Suorineni F, Su K. A study on the dynamic behavior of the Meuse/Haute-Marne argillite. *Physics and Chemistry of the Earth, Parts A/B/C.* 2007;32(8): 907-916.
58. Li Y, Xia C. Time-dependent tests on intact rocks in uniaxial compression. *Int J Rock Mech Min Sci.* 2000;37(3): 467-475.
59. Sylven ET, Agarwal S, Briant CL, Cleveland RO. High strain rate testing of kidney stones. *J Mater Sci Mater Med.* 2004;15(5): 613-617.
60. Lindholm U, Yeakley L, Nagy A. The dynamic strength and fracture properties of dresser basalt. *International Journal of Rock Mechanics and Mining Sciences & Geomechanics Abstracts.* 1974;11(5): 181-191.
61. Xia K, Nasseri MHB, Mohanty B, Lu F, Chen R, Luo SN. Effects of microstructures on dynamic compression of Barre granite. *Int J Rock Mech Min Sci.* 2008;45(6): 879-887.
62. Goldsmith W, Sackman J, Ewerts C. Static and dynamic fracture strength of Barre granite. *International Journal of Rock Mechanics and Mining Sciences & Geomechanics Abstracts.* 1976;13(11): 303-309.
63. Olsson W. The compressive strength of tuff as a function of strain rate from 10< sup>− 6</sup> to 10< sup> 3</sup>/sec. *International Journal of Rock Mechanics and Mining Sciences & Geomechanics Abstracts.* 1991;28(1): 115-118.
64. Zou C, Wong LNY. Size and geometry effects on the mechanical properties of Carrara marble under dynamic loadings. *Rock Mech Rock Eng.* 2016;49(5): 1695-1708.
65. Wong LNY, Zou C, Cheng Y. Fracturing and failure behavior of Carrara marble in quasistatic and dynamic brazilian disc tests. *Rock Mech Rock Eng.* 2014;47(4): 1117-1133.
66. Brace WF, Bombolakis EG. A note on brittle crack growth in compression. *J Geophys Res.* 1963;68(12): 3709-3713.
67. Lajtai EZ. Brittle fracture in compression. *Int J Fract.* 1974;10(4): 525-536.
68. Einstein HH, Stephansson O. Fracture systems, fracture propagation and coalescence. *Geoeng2000-An International Conference on Geotechnical & Geological Engineering.* Melbourne, Australia: International Society for Rock Mechanics; 2000:1-41.
69. Wong LNY, Einstein HH. Systematic evaluation of cracking behavior in specimens containing single flaws under uniaxial compression. *Int J Rock Mech Min Sci.* 2009;46(Compendex): 239-249.
70. Atkinson BK. Subcritical crack growth in geological materials. *Journal of Geophysical Research: Solid Earth.* 1984;89(B6): 4077-4114.
71. Bobet A, Einstein HH. Fracture coalescence in rock-type materials under uniaxial and biaxial compression. *Int J Rock Mech Min Sci.* 1998;35(7): 863-888.
72. Yang S-Q, Huang Y-H, Tian W-L, Zhu J-B. An experimental investigation on strength, deformation and crack evolution behavior of sandstone containing two oval flaws under uniaxial compression. *Eng Geol.* 2017;217(C): 35-48.
73. Hazzard JF, Young RP, Maxwell SC. Micromechanical modeling of cracking and failure in brittle rocks. *Journal of Geophysical Research: Solid Earth.* 2000;105(B7): 16683-16697.

74. Kazerani T, Zhao GF, Zhao J. Dynamic fracturing simulation of brittle material using the distinct lattice spring method with a full rate-dependent cohesive law. *Rock Mech Rock Eng*. 2010;43(6): 717-726.
75. Cai X, Liu W, Shen X, Gao Y. Flow-coupled cohesive interface framework for simulating heterogeneous crack morphology and resolving numerical divergence in hydraulic fracture. *Extreme Mech Lett.* 2021;45: 101281.
76. Zhao J, Li HB, Wu MB, Li TJ. Dynamic uniaxial compression tests on a granite. *Int J Rock Mech Min Sci.* 1999;36(2): 273-277.
77. Zhao J. Applicability of Mohr–Coulomb and Hoek–Brown strength criteria to the dynamic strength of brittle rock. *Int J Rock Mech Min Sci.* 2000;37(7): 1115-1121.